

Article

# Synthesis and Physical Properties of Tetrathiafulvalene-8-Quinolinato Zinc(II) and Nickel(II) Complexes

Keihiro Tsujimoto, Shinya Yamamoto and Hideki Fujiwara \* 

Department of Chemistry, Graduate School of Science, Osaka Prefecture University, Gakuen-cho, Naka-ku, Sakai 599-8531, Japan; kjiro.t@gmail.com (K.T.); shinya.y12@gmail.com (S.Y.)

\* Correspondence: hfujii@c.s.osakafu-u.ac.jp; Tel./Fax: +81-72-254-9818

**Abstract:** To develop donor–acceptor–donor (D–A–D) type new photo-electric conversion materials, new tetrathiafulvalene (TTF)-Mq<sub>2</sub>-TTF complexes **1** and **2** were synthesized, where two bis(*n*-hexylthio)tetrathiafulvalene moieties were attached to the Mq<sub>2</sub> part (**1**: M = Zn, **2**: M = Ni, q = 8-quinolinato) through amide bonds. UV-Vis absorption spectra of these complexes showed strong and sharp absorption maxima at 268 nm and small absorption maxima around 410 nm, corresponding to those of Znq<sub>2</sub> and Niq<sub>2</sub> parts. Furthermore, complexes **1** and **2** exhibited absorption tails up to a much longer wavelength region of ca. 700 nm, suggesting the appearance of charge transfer absorption from TTF to the Mq<sub>2</sub> parts. The photoelectrochemical measurements on the thin films of these complexes casted on ITO-coated glass substrates suggest that positive photocurrents can be generated by the photoinduced intramolecular electron transfer process between the TTF and Mq<sub>2</sub> parts.

**Keywords:** tetrathiafulvalene; photofunctional materials; optical properties; photoelectric conversion



**Citation:** Tsujimoto, K.; Yamamoto, S.; Fujiwara, H. Synthesis and Physical Properties of Tetrathiafulvalene-8-Quinolinato Zinc(II) and Nickel(II) Complexes. *Inorganics* **2021**, *9*, 11. <https://doi.org/10.3390/inorganics9020011>

Academic Editor: Martin T. Lemaire  
Received: 25 December 2020  
Accepted: 26 January 2021  
Published: 1 February 2021

**Publisher's Note:** MDPI stays neutral with regard to jurisdictional claims in published maps and institutional affiliations.



**Copyright:** © 2021 by the authors. Licensee MDPI, Basel, Switzerland. This article is an open access article distributed under the terms and conditions of the Creative Commons Attribution (CC BY) license (<https://creativecommons.org/licenses/by/4.0/>).

## 1. Introduction

In the recent studies of organic functional materials based on tetrathiafulvalene (TTF) derivatives, donor–acceptor (D–A) type dyads have attracted much interest in the fields of optoelectronic materials. Particularly, photoinduced intramolecular electron transfer (PET) process between electron-donating TTF derivatives (D) and electron-accepting parts (A) such as fluorophores, C<sub>60</sub> and chelating ligands has yielded several photofunctional materials such as chemical sensors based on fluorescence probe functionalities, organic photovoltaic (OPV) cells and nonlinear optical devices [1–7]. Among them, to develop photoinduced conducting materials and photo-electric conversion materials, we have investigated the photofunctional materials using the TTF-based D–A type dyads containing strongly fluorescent parts such as 2, 5-diphenyl-1, 3, 4-oxadiazole (PPD) [8,9], 1, 3-benzothiazole (BTA) [10–12], fluorene [13,14] and 4, 4-difluoro-4-bora-3a, 4a-diaza-s-indacene (BODIPY) [15,16] as antennas for photoexcitation. On the other hand, since the first fabrication of organic light-emitting diodes (OLEDs) using tris(8-quinolinato)aluminum (Alq<sub>3</sub>, q = 8-quinolinato) [17], various kinds of 8-quinolinato transition metal complexes Mq<sub>x</sub> have attracted much attention because of their strongly fluorescent character, high thermal stability and excellent electron transport properties [18–22]. Furthermore, Alq<sub>3</sub> is reported to improve the conversion efficiency of heterojunction OPV cells by acting as a photosensitizer and buffer material [23,24]. Therefore, we focused on the Mq<sub>x</sub> complexes as a photofunctional A part and we designed new D–A–D type complexes containing TTF derivatives and Mq<sub>2</sub> part to realize new photo-electric conversion materials. In such transition metal complexes, substitution of the central metal atom would bring about the geometrical change around the central metal atom and the resultant changes in their electronic properties. In this paper, we report the synthesis, spectroscopic studies and photo-electric conversion functionality of TTF-Mq<sub>2</sub>-TTF complexes (**1**: M = Zn, **2**: M = Ni, q = 8-quinolinato, Chart 1) with amide bonds as spacers.

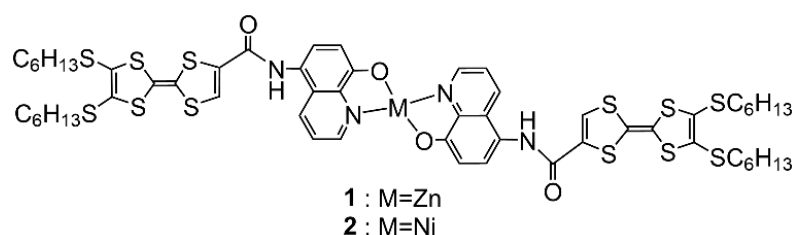
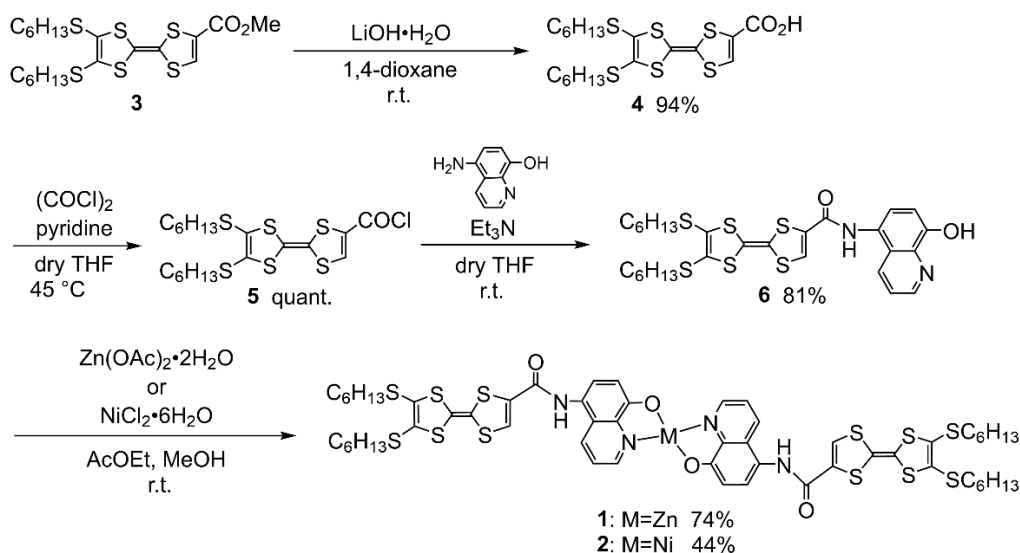


**Chart 1.** Molecular structure of complexes **1** and **2**.

## 2. Results and Discussion

### 2.1. Synthesis

Synthesis of transition metal complexes **1** and **2** was performed according to Scheme 1. Thus, TTF derivative **3** containing one methoxycarbonyl group and two *n*-hexylthio groups was synthesized by following the reported method [25]. We introduced two *n*-hexylthio groups to improve the solubility of the target complexes **1** and **2**. Compound **3** was hydrolyzed into the corresponding carboxylic acid **4** using an excess of lithium hydroxide monohydrate in 1,4-dioxane at room temperature [26]. Then, carboxylic acid **4** was converted into its acid chloride **5** by the reaction with oxalyl chloride and a catalytic amount of pyridine in THF [27]. Ligand **6**, containing an 8-hydroxyquinoline part, was obtained in 81% yield by the reaction between **5** and 5-amino-8-hydroxyquinoline hydrochloride in the presence of triethylamine in dry THF at room temperature [28]. The target transition metal complexes **1** (M = Zn) and **2** (M = Ni) were prepared by the reaction of ligand **6** with the corresponding metal compounds, zinc (II) acetate dihydrate or nickel (II) chloride hexahydrate in the mixture of methanol and ethyl acetate at room temperature in 74% and 44% yields, respectively.



**Scheme 1.** Synthesis of transition metal complexes **1** and **2**.

### 2.2. Electrochemical Properties of **1** and **2**

Electrochemical properties of complexes **1** and **2** were investigated by cyclic voltammetry technique in benzonitrile at 25 °C together with those of bis(methylthio)-TTF (BTM-TTF) and  $Mq_2$  (M = Zn, Ni). Complexes **1** and **2** showed two pairs of one-electron reversible redox waves at oxidation side ( $E_{ox1}$  and  $E_{ox2}$ ) and irreversible one at reduction side ( $E_{red}$ ) as summarized in Table 1. Because two pairs of one-electron reversible redox waves were also observed in BTM-TTF (+0.48 V and +0.82 V vs. Ag/AgCl), the first and second oxidations of complexes **1** and **2** are assigned to the oxidation processes at the bis(*n*-hexylthio)-TTF

part, although these redox potentials ( $E_{ox1}$  and  $E_{ox2}$ ) of complexes **1** and **2** suggest their lower electron-donating ability than that of BTM-TTF due to the substitution by an electron-withdrawing amide part. In comparison to the redox potentials of  $Znq_2$  or  $Niq_2$ , it is found that the reduction process ( $E_{red}$ ) of complexes **1** and **2** occurs at the  $Mq_2$  parts around ca.  $-1.2$  V vs. Ag/AgCl.

**Table 1.** Redox potentials (V) of **1**, **2**, BTM-TTF,  $Znq_2$  and  $Niq_2$  <sup>a</sup>.

Compound	$E_{red}$	$E_{ox1}$	$E_{ox2}$	$E_2 - 1 E_1$
<b>1</b> (M = Zn)	$-1.19^b$	+0.56	+0.92	0.36
<b>2</b> (M = Ni)	$-1.16^b$	+0.59	+0.90	0.31
BTM-TTF		+0.48	+0.82	0.34
$Znq_2$	$-1.17^b$			
$Niq_2$	$-1.02^b$			

<sup>a</sup> V vs. Ag/AgCl,  $0.1 \text{ mol L}^{-1}$   $n\text{-Bu}_4\text{NClO}_4$  in benzonitrile at  $25^\circ\text{C}$ , Pt electrodes, scan rate of  $50 \text{ mV s}^{-1}$ . The potentials were corrected with Ferrocene;  $E(\text{Fc}/\text{Fc}^+) = +0.48$  V vs. Ag/AgCl. <sup>b</sup> Irreversible step.

### 2.3. UV-Vis Absorption Spectra and Emission Spectra

UV-Vis absorption spectra were measured using  $10^{-4}$  M DMF solutions at room temperature as shown in Figure 1. As well as the case of  $Znq_2$  and  $Niq_2$ , complexes **1** and **2** containing TTF parts also showed almost the same spectra to each other, and gave strong and sharp absorption maxima at 268 nm and small absorption maxima around 410 nm, which just correspond to those of  $Znq_2$  ( $\lambda_{max} = 268 \text{ nm}$ , 400 nm) and  $Niq_2$  ( $\lambda_{max} = 268 \text{ nm}$ , 416 nm) (see Table 2). Furthermore, weak maxima around 320 nm corresponding to that of TTF ( $\lambda_{max} = 312 \text{ nm}$ ) were also observed in complexes **1** and **2**. On the other hand, although  $Znq_2$  and  $Niq_2$  showed absorption tails up to around 470 nm, complexes **1** and **2** exhibited their absorption tails up to a much longer wavelength region of around 700 nm, which suggests the appearance of a charge transfer (CT) absorption band from the TTF to  $Mq_2$  parts and is preferable for the photo-electric conversion by visible light. Emission spectra of the  $10^{-6}$  M  $\text{CHCl}_3$  solution of complexes **1** and **2**,  $Znq_2$  and  $Niq_2$  were measured at room temperature under identical conditions (see Supplementary Materials Figure S1). When the solutions of these complexes were irradiated by an excitation light of 268 nm that corresponds to their absorption maxima (strong  $\pi\text{-}\pi^*$  transitions of the  $Mq_2$  part), strong fluorescences were observed at around 404 nm. The intensities of fluorescences of complexes **1** and **2** were of almost the same degree as the corresponding  $Mq_2$  (M = Zn, Ni) complexes, suggesting that almost no suppression of fluorescence occurred due to weak intramolecular CT interaction between the TTF and  $Mq_2$  complex parts.

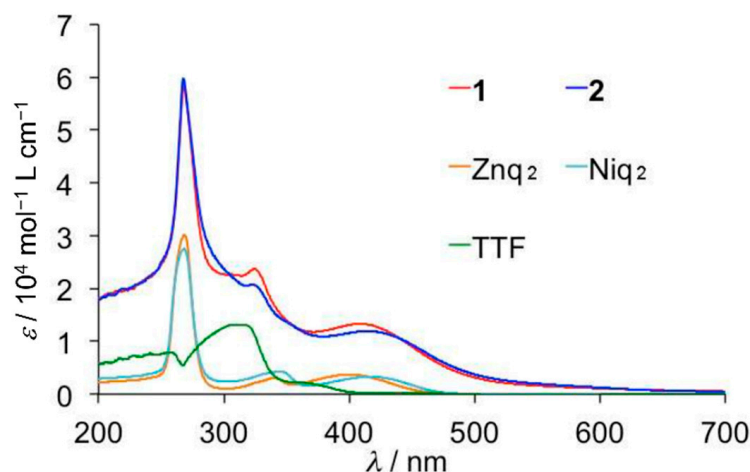


**Figure 1.** UV-Vis absorption spectra in  $10^{-4}$  M DMF solutions.

**Table 2.** Wavelength of maximum absorption peaks ( $\lambda_{\max}$ ), absorption coefficients at 268 nm ( $\epsilon$ ) and emission peaks ( $\lambda_{\text{em}}$ ) under excitation light of 268 nm.

Compound	$\lambda_{\max}$ (nm)	$\epsilon$ ( $10^4 \text{ mol}^{-1} \text{ L cm}^{-1}$ )	$\lambda_{\text{em}}$ (nm)
<b>1</b> (M = Zn)	268, 323, 402	5.1	404
<b>2</b> (M = Ni)	268, 322, 405	4.5	404
TTF	312	1.3	
Znq <sub>2</sub>	268, 340, 400	3.9	404
Niq <sub>2</sub>	268, 342, 416	3.6	404

#### 2.4. Molecular Orbital Calculation

Because single crystalline samples of complexes **1** and **2** were not obtained, molecular structures of these complexes in their isolated states are estimated by the DFT calculation at the B3LYP level using the LANL2DZ basis set for the central zinc and nickel atoms and the 6-31G(d, p) basis set for the other atoms (GAUSSIAN 09 package), as shown in Figure 2 [29]. In the optimization of molecular structures, the *n*-hexylthio substituents on the TTF part are removed. The optimized molecular structure of Zn complex **1** shows distorted tetrahedral coordination around the central zinc atom with a dihedral angle of 85.1° between two 8-quinolinato ligands. Therefore, two TTF-8-quinolinato ligands are largely twisted to each other on the central zinc atom. Furthermore, the dihedral angles between the 1,3-dithiole rings that connect to the amide bond and 8-quinolinato parts are 20.1° and 49.7°, suggesting that the intramolecular interaction between the TTF part and Znq<sub>2</sub> part may be weakened by these twisted structures around the amide bonds. Such a largely twisted structure of the amide-containing TTF-*N*-heterocyclic ligand was reported in the bipyridine derivative (dihedral angle: 38.9°) [28]. On the other hand, Ni complex **2** shows square-planar coordination around the central nickel atom and the Niq<sub>2</sub> part has almost complete planarity, as shown in Figure 2b. Such a planar structure has been reported in bis(7-isopropyl-8-quinolinato)nickel(II) complex and bis-(4-methylpyridine)bis(8-quinolinolato)nickel(II) complex [30,31]. Because the dihedral angles between the 1,3-dithiole rings that connect to the amide bond and 8-quinolinato parts are calculated to be 8.6° and 11.6° in complex **2**, the intramolecular interaction between the TTF and Niq<sub>2</sub> parts is considered to be stronger through more planar structures of TTF-8-quinolinato ligands around the amide bonds than Zn complex **1**. Such a relatively planar structure of the amide-containing TTF-*N*-heterocyclic ligand was also reported in the symmetric D-A-D type bipyridine derivative (dihedral angle: 9.6°) [28]. These deviations about the dihedral angles between the 1,3-dithiole rings and *N*-heterocyclic parts suggest the structural flexibility around the amide bond.

In these complexes, HOMO and HOMO-1 orbitals are almost degenerated to each other and localized on the TTF parts, whereas LUMO and LUMO+1 orbitals are localized on the 8-quinolinato ligands, as shown in Figures S2 and S3. The HOMO-LUMO gap energies of complexes **1** and **2** are estimated to be 2.96 eV and 2.60 eV from the energy levels of HOMO and LUMO orbitals (**1**; HOMO: -4.93 eV, LUMO: -1.97 eV, **2**; HOMO: -4.79 eV, LUMO: -2.19 eV). Although these results of the molecular orbital calculations of complexes **1** and **2** in their isolated states suggest different electronic structures from each other owing to their different coordination geometries (see the simulated UV-Vis spectra in Figure S4), the observed optical spectra and redox potentials of these complexes measured in their solution states are almost the same as each other (see Figure 1), suggesting that these complexes may adopt almost the same molecular structure by solvation in polar solvents such as benzonitrile and DMF. Actually, the Znq<sub>2</sub> complex was reported to adopt a square-planar coordination around the central zinc atom when two water or two DMSO molecules were axially coordinated to the Znq<sub>2</sub> complex [32-34].

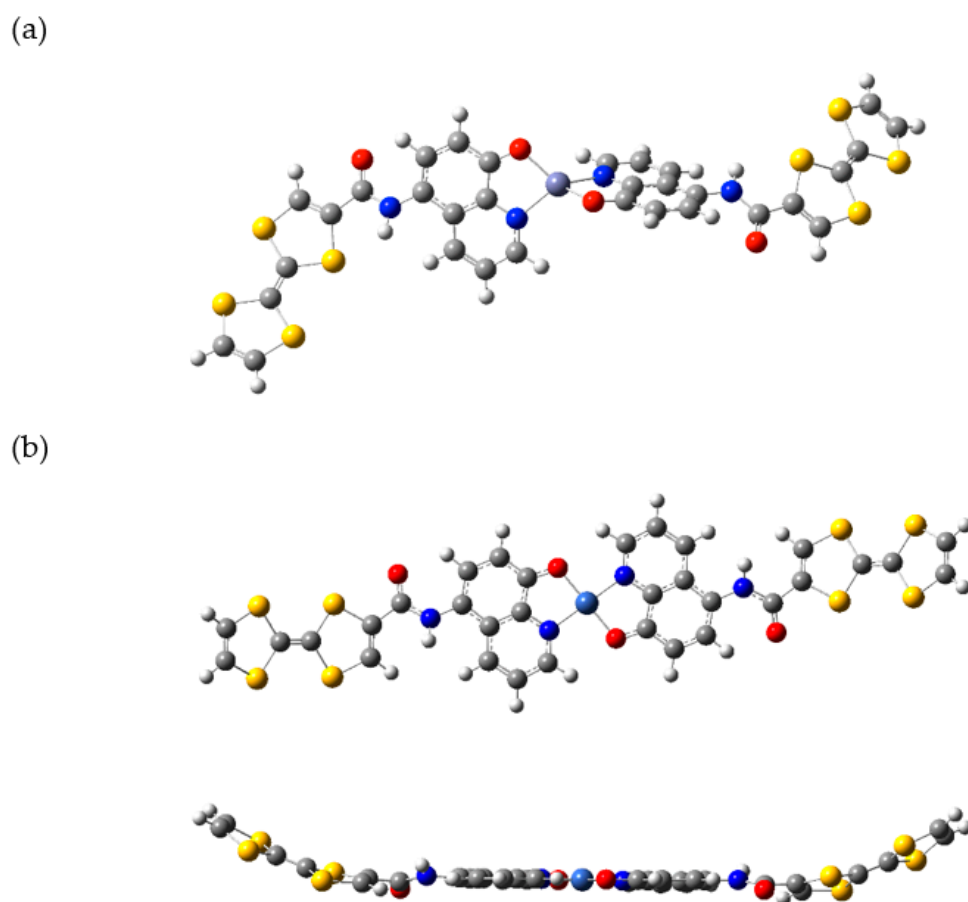


**Figure 2.** Optimized molecular structures of (a) Zn complex **1** and (b) Ni complex **2** in their isolated states on the basis of DFT method (B3LYP/LANL2DZ for transition metals and B3LYP/6–31G(d,p) for the other atoms).

### 2.5. Photoelectric Conversion Functionalities of Thin Films

To estimate the photo-electric conversion functionality of complexes **1** and **2**, photocurrent measurements were performed on their thin film samples by a photoelectrochemical method. Thin film samples of complexes were prepared by a casting method as follows: 10  $\mu\text{L}$  of 1 g  $\text{L}^{-1}$  DMSO solution of the complexes was casted on an ITO-coated soda-lime glass substrate (Aldrich No. 576352; 1.0 cm  $\times$  0.8 cm) and was dried in vacuo at 30  $^{\circ}\text{C}$  for 1h. Photoelectrochemical measurements were performed in 0.5 mol  $\text{L}^{-1}$  aqueous KCl solution using these thin film-coated ITO electrodes as a working electrode, and platinum and Ag/AgCl electrodes were used as counter and reference electrodes, respectively. Under irradiation from a 150 W Xe lamp, generated photocurrents between the working and counter electrodes were recorded in the wavelength range from 300 to 600 nm under bias voltage vs. Ag/AgCl reference electrode. As shown in Figure 3, cathodic photocurrent maxima of 622 nA under  $-0.2$  V, 265 nA under 0 V of bias voltage vs. Ag/AgCl electrode at 334 nm for **1**, 522 nA under  $-0.2$  V, 163 nA under 0 V of bias voltage vs. Ag/AgCl electrode at 325 nm for **2**, were observed, corresponding to the absorption maxima of the identical thin film samples on the ITO electrode. These results suggest that the photons absorbed by these complexes were converted to electric currents on the ITO electrode. Because no photocurrent generation was observed in the cases of thin films of only TTF or only  $\text{Mq}_2$  ( $\text{M} = \text{Zn}, \text{Ni}$ ), the observation of such positive photocurrents suggests that photons absorbed by complexes **1** and **2** were converted into electric currents as a result of a photo-induced intramolecular electron transfer process between the TTF and  $\text{Mq}_2$  parts.

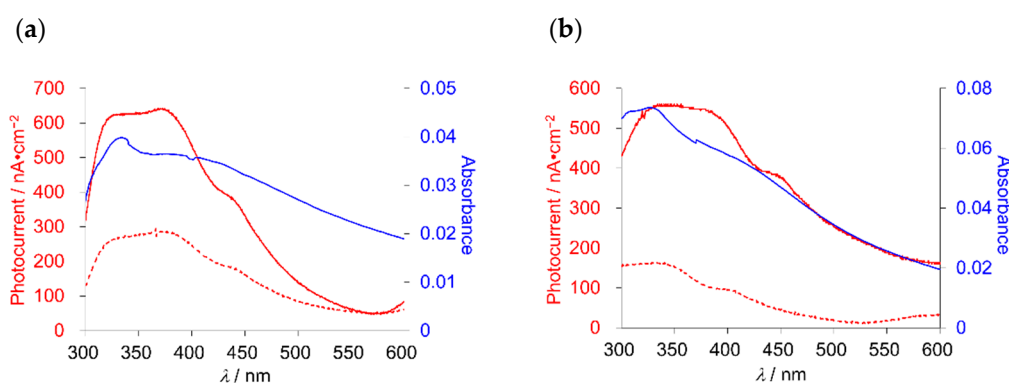


**Figure 3.** Photocurrent action spectra under the bias voltage vs. Ag/AgCl reference electrode (red solid line:  $-0.2$  V, red dashed line:  $0$  V vs. Ag/AgCl) and absorption spectra (blue line) of the thin film samples of (a) Zn complex **1** and (b) Ni complex **2** prepared by a casting method on the ITO electrodes.

The maximum efficiencies of photo-electric conversion ( $\eta_{\max}$ ) under  $-0.2$  V vs. Ag/AgCl electrode were calculated to be 0.23% at 334 nm for **1** and 0.14% at 325 nm for **2**, from values of maximum photocurrent per 1 cm<sup>2</sup> thin film samples ( $I_{\max}/A\text{ cm}^{-2}$ ), absorbance of the thin film used ( $Abs$ ), power of irradiated light ( $W/W\text{ cm}^{-2}$ ) at wavelength  $\lambda$  nm as summarized in Table 3 using an equation as follows;  $\eta_{\max} = [\text{number of generated photoelectrons } (I_{\max}/e)] / [\text{number of absorbed photons } [(1-10^{-Abs})W\lambda/hc]]$  where  $e$  is the elementary charge of an electron,  $h$  is Planck's constant and  $c$  is the velocity of light [35]. Because these cathodic (positive) photocurrents increase with increasing negative bias voltage from  $0$  V to  $-0.2$  V, the application of negative bias voltage promotes the electron transfer process from the ITO electrode to the holes generated on the complexes upon irradiation. These enhancement phenomena by the application of negative bias voltage are almost the same as those of the other TTF-based dyads studied so far [8,14,15]; however, the degrees of conversion efficiency of complexes **1** and **2** ( $\sim 0.2\%$ ) are a little smaller than our previously reported values ( $1.5\sim 0.5\%$ ), probably due to the weak intramolecular CT interaction in complexes **1** and **2** with  $\sigma$ -bonded amide spacers.

**Table 3.** Estimation of maximum photoelectric conversion efficiency ( $\eta_{\max}$ ) of the thin film samples of complexes **1** and **2**.

Compound	Bias Voltage vs. Ag/AgCl (V)	Maximum Photocurrent ( $I_{\max}/\text{nA cm}^{-2}$ )	Light Power ( $W/\text{mW cm}^{-2}$ )	$\lambda$ (nm)	Absorbance of Thin Film ( $Abs$ )	$\eta_{\max}$ (%)
<b>1</b>	$0$	265	11.4	334	0.040	0.099
<b>1</b>	$-0.2$	622	11.4	334	0.040	0.23
<b>2</b>	$0$	163	9.2	325	0.073	0.044
<b>2</b>	$-0.2$	522	9.2	325	0.073	0.14

### 3. Conclusions

We have synthesized new TTF-Mq<sub>2</sub>-TTF complexes (**1**: M = Zn, **2**: M = Ni, q = 8-quinolinato) with amide bonds as spacers to develop D–A–D type new photo-electric conversion materials. UV-Vis absorption spectra of these complexes showed strong and sharp absorption maxima at 268 nm and small absorption maxima around 410 nm, corresponding to those of Znq<sub>2</sub> and Niq<sub>2</sub> parts, together with weak maxima around 320 nm, corresponding to that of TTF. Furthermore, complexes **1** and **2** exhibited absorption tails up to much longer wavelength region of ca. 700 nm, suggesting the appearance of charge transfer absorption from TTF to the Mq<sub>2</sub> parts. The photoelectrochemical measurements on the thin films of these complexes suggest that positive photocurrents can be generated by the photo-induced intramolecular electron transfer process between the TTF and Mnq<sub>2</sub> parts of the complexes. We are now engaging in the modification of molecular structures

of complexes by introducing  $\pi$ -spacers such as oligothiophenes into the spacer part to enhance the intramolecular CT interaction.

## 4. Materials and Methods

### 4.1. General

THF was freshly distilled under  $N_2$  over sodium/benzophenone. Other chemical reagents were purchased and used without further purification. NMR spectra were recorded using JEOL JNM-AL400 400 MHz spectrometer (Akishima, Tokyo, Japan) and Varian 400-MR 400 MHz spectrometer (Hachioji, Tokyo, Japan). High-resolution mass spectra (HRMS) using EI and FAB<sup>+</sup> methods were measured using a JEOL JMS-700 mass spectrometer (Akishima, Tokyo, Japan). IR spectra were recorded on KBr pellets using a JASCO FT/IR-4100 spectrometer (Hachioji, Tokyo, Japan). UV-Visible absorption spectra were measured using a JASCO V-670 UV-VIS spectrophotometer (Hachioji, Tokyo, Japan). Cyclic voltammograms were measured using a BAS Electrochemical Analyzer Model 612B (Sumida-ku, Tokyo, Japan). Elemental analyses of both metal complexes were performed using Perkin Elmer Series II analyzer 2400 (Yokohama, Kanagawa, Japan).

### 4.2. Synthesis

**Compound 4** [26]. An aqueous solution of LiOH·H<sub>2</sub>O (0.88 g, 21 mmol in 10 mL water) was added to a stirred solution of compound 3 [25] (2.1 g, 4.2 mmol) in 1,4-dioxane (60 mL) at room temperature under nitrogen. After stirring for 21 h, 5 M HCl aq. (5.0 mL, 25 mmol) was added and the solution stirred for a few minutes. After adding water until the pH of water phase reached 1–2, the organic phase was extracted with diethyl ether and dried over anhydrous magnesium sulfate. After filtration of drying reagent, the filtrate was evaporated in vacuo, and the residue was purified by column chromatography on silica gel with methanol/dichloromethane mixed solvent ( $R_f = 0.2$ ) as an eluent. After evaporation of solvents, red solid 4 (1.9 g, 4.0 mmol) was obtained in 94% yield. mp. 117–118 °C (dec.); <sup>1</sup>H-NMR (400 MHz, CDCl<sub>3</sub>)  $\delta$  7.48 (s, 1H), 2.81 (m, 4H), 1.63 (quintet,  $J = 7.2$  Hz, 4H), 1.41 (quintet,  $J = 7.2$  Hz, 4H), 1.30 (m, 8H), 0.89 (t,  $J = 7.2$  Hz, 6H); IR (KBr)  $\nu$  (cm<sup>-1</sup>) 725, 803, 1023, 1097, 1262, 1287, 1416, 1525, 1560, 1675, 2854, 2922, 2952; EI-HRMS  $m/z$  calcd for C<sub>19</sub>H<sub>28</sub>O<sub>2</sub>S<sub>6</sub>: 480.0414; found: 480.0327 (M<sup>+</sup>).

**Compound 5** [27]. Oxalyl chloride (1.0 mL, 12 mmol) and a catalytic amount of pyridine (3.0  $\mu$ L) were added to a stirred dry THF solution (80 mL) containing compound 4 (1.9 g, 4.0 mmol) under nitrogen at 45 °C and the mixture was stirred for 2 h. After evaporation of solvents, black purple oil of crude 5 (2.2 g) was obtained and used for the next reaction without further purification. <sup>1</sup>H-NMR (400 MHz, CDCl<sub>3</sub>)  $\delta$  7.77 (s, 1H), 2.82 (br, 4H), 1.61–1.65 (m, 4H), 1.42 (quintet,  $J = 7.2$  Hz, 4H), 1.26–1.29 (m, 8H), 0.91 (t,  $J = 7.2$  Hz, 6H); IR (KBr)  $\nu$  (cm<sup>-1</sup>) 651, 723, 756, 850, 1144, 1209, 1463, 1521, 1158, 1729, 2855, 2926, 2954; FAB-HRMS (Matrix: 3-nitrobenzyl alcohol)  $m/z$  calcd for C<sub>28</sub>H<sub>34</sub>N<sub>2</sub>O<sub>2</sub>S<sub>6</sub>: 498.0075; found: 498.0053 (M<sup>+</sup>).

**Compound 6**. Dry THF (50 mL) solution of crude compound 5 (1.8 g, 3.6 mmol) was added dropwise to dry THF (70 mL) solution of 5-amino-8-hydroxyquinoline dihydrochloride (1.3 g, 5.4 mmol) for 15 min under nitrogen. Then, triethylamine (11 mL, 79 mmol) was added and the reaction mixture was stirred for 15 h at room temperature. Thereafter, the solvent was removed under reduced pressure and the residue was dissolved in dichloromethane and washed with brine. The organic phase was washed with water and dried over anhydrous magnesium sulfate. After filtration of drying reagent and evaporation of solvents under reduced pressure, thick black solid of crude 6 (1.8 g, 2.9 mmol) was obtained in 81% yield and used for the next reaction without further purification. <sup>1</sup>H-NMR (400 MHz, CDCl<sub>3</sub>)  $\delta$  8.81 (s, 1H), 8.14 (d,  $J = 8.3$  Hz, 1H), 7.52 (d,  $J = 8.3$  Hz, 1H), 7.50 (s, 1H), 7.50–7.30 (m, 1H), 7.15 (d,  $J = 8.0$  Hz, 1H), 2.83 (t,  $J = 7.3$  Hz, 4H), 1.64 (quintet,  $J = 7.3$  Hz, 4H), 1.40 (m, 4H), 1.31 (m, 8H), 0.90 (m, 6H); IR (KBr)  $\nu$  (cm<sup>-1</sup>) 700, 723, 775, 815, 882, 1018, 1196, 1231, 1263, 1285, 1374, 1418, 1474, 1501, 1536, 1563, 1614, 2852, 2924,

2953; FAB-HRMS (Matrix: 3-nitrobenzyl alcohol)  $m/z$  calcd for  $C_{28}H_{34}N_2O_2S_6$ : 622.0945; found: 622.0951 ( $M^+$ ).

Zn complex **1**. Zinc (II) acetate dihydrate (0.11 g, 0.48 mmol) in methanol (10 mL) was added dropwise to a stirred ethyl acetate (30 mL) solution of compound **6** (0.30 g, 0.48 mmol) under nitrogen. After stirring at room temperature for 1h, brownish yellow precipitation was filtered and washed with methanol and ethyl acetate, then dried in vacuo to obtain Zn complex **1** in 74% yield. mp.  $>300$  °C;  $^1H$ -NMR (400 MHz, DMSO- $d_6$ )  $\delta$  10.16 (s, 2H), 8.5–8.8 (m, 2H), 8.2–8.3 (m, 2H), 7.85 (s, 2H), 7.6–7.7 (m, 2H), 7.25–7.35 (m, 2H), 6.7–6.8 (m, 2H), 2.8–2.9 (m, 8H), 1.5–1.6 (m, 8H), 1.3–1.4 (m, 8H), 1.2–1.3 (m, 16H), 0.8–0.9 (m, 12H); IR (KBr)  $\nu$  ( $cm^{-1}$ ) 724, 785, 1101, 1241, 1285, 1325, 1387, 1407, 1466, 1499, 1576, 1651, 2853, 2925, 2953; Calcd for  $C_{56}H_{66}N_4O_4S_{12}Zn$ : C, 51.37; H, 5.08; N, 4.28. Found: C, 51.08; H, 5.19; N, 4.12; FAB-HRMS (Matrix: 3-nitrobenzyl alcohol)  $m/z$  calcd for  $C_{56}H_{66}N_4O_4S_{12}Zn$ : 1306.1024; Found: 1306.0996 ( $M^+$ ).

Ni complex **2** was synthesized in 44% yield by the same method as Zn complex **1** using nickel (II) dichloride hexahydrate. mp  $>300$  °C; IR (KBr)  $\nu$  ( $cm^{-1}$ ) 722, 781, 819, 1094, 1283, 1376, 1407, 1466, 1507, 1558, 1646, 2854, 2925, 2954; Calcd for  $C_{56}H_{66}N_4O_4S_{12}Ni$ : C, 51.64; H, 5.11; N, 4.30. Found: C, 51.37; H, 5.18; N, 4.45; FAB-HRMS (Matrix: 3-nitrobenzyl alcohol)  $m/z$  calcd for  $C_{56}H_{66}N_4O_4S_{12}Ni$ : 1300.1086; Found: 1301.1085 ( $M^+$ ). Because any resonance signal of protons could not be observed in the  $^1H$ -NMR spectrum of Ni complex **2**, the  $Ni^{2+}$  species of complex **2** is considered to be in paramagnetic  $S = 1$  high spin state of the  $d^8$  electron configuration. Several  $NiQ_2$  complexes have been reported to be paramagnetic [36]. The magnetic properties of the Ni complex will be discussed in the future papers.

**Supplementary Materials:** The following are available online at <https://www.mdpi.com/2304-6740/9/2/11/s1> as a separate electronic file in PDF format, emission spectra of complexes **1** and **2**,  $ZnQ_2$  and  $NiQ_2$ , molecular orbital calculation of complexes **1** and **2** on the basis of the DFT theory, UV-Vis simulated spectra of **1** and **2** calculated on the basis of a TD-DFT method and NMR charts of compounds **4**, **5**, **6** and Zn complex **1**. Figure S1: Emission spectra of the  $10^{-6}$  M  $CHCl_3$  solution of complexes **1** and **2**,  $ZnQ_2$  and  $NiQ_2$  measured at room temperature under the identical conditions using an excitation light of 268 nm; Figure S2: Molecular orbitals and energy levels of Zn complex **1**; Figure S3: Molecular orbitals and energy levels of Ni complex **2**; Figure S4: UV-Vis simulated spectra of **1** and **2** calculated on the basis of a TD-DFT method.

**Author Contributions:** Conceptualization, H.F.; methodology, H.F.; investigation, K.T., S.Y. and H.F.; writing—original draft preparation, K.T. and H.F.; writing—review and editing, H.F.; funding acquisition, H.F. All authors have read and agreed to the published version of the manuscript.

**Funding:** This research was funded in part by Grants-in-Aid for Scientific Research (No. 20110006 and No. 21750150) from the Ministry of Education, Culture, Sports, Science and Technology of Japan, and by a Grant for Young Researchers from the JGC-S Scholarship Foundation.

**Institutional Review Board Statement:** Not applicable.

**Informed Consent Statement:** Not applicable.

**Data Availability Statement:** Data is contained within the article and supplementary material.

**Conflicts of Interest:** The authors declare no conflict of interest.

## References

1. Brunetti, F.G.; Lopez, J.L.; Atienza, C.; Martin, N.  $\pi$ -Extended TTF: A versatile molecule for organic electronics. *J. Mater. Chem.* **2012**, *22*, 4188–4205. [CrossRef]
2. Gorgues, A.; Hudhomme, P.; Salle, M. Highly functionalized tetrathiafulvalenes: Riding along the synthetic trail from electrophilic alkynes. *Chem. Rev.* **2004**, *104*, 5151–5184. [CrossRef] [PubMed]
3. Segura, J.L.; Martin, N. New concepts in tetrathiafulvalene chemistry. *Angew. Chem. Int. Ed. Engl.* **2001**, *40*, 1372–1409. [CrossRef]
4. Wenger, S.; Bouit, P.-A.; Chen, Q.; Teuscher, J.; Censo, D.D.; Humphry-Baker, R.; Moser, J.-E.; Delgado, J.L.; Martín, N.; Zakeeruddin, S.M.; et al. Efficient Electron Transfer and Sensitizer Regeneration in Stable  $\pi$ -Extended Tetrathiafulvalene-Sensitized Solar Cells. *J. Am. Chem. Soc.* **2010**, *132*, 5164–5169. [CrossRef] [PubMed]

5. Yamada, J.; Sugimoto, T. *TTF Chemistry: Fundamentals and Applications of Tetrathiafulvalene*; Kodansha-Springer: Tokyo, Japan, 2004.
6. Biswas, C.; Katturi, N.K.; Duvva, N.; Giribabu, L.; Soma, V.R.; Raavi, S.S.K. Multistep Electron Injection Dynamics and Optical Nonlinearity Investigations of  $\pi$ -Extended Thioalkyl-Substituted Tetrathiafulvalene Sensitizers. *J. Phys. Chem. C* **2020**, *124*, 24039–24051. [[CrossRef](#)]
7. Mogensen, J.; Michaels, H.; Roy, R.; Broløs, L.; Kilde, M.D.; Freitag, M.; Nielsen, M.B. Indenofluorene-Extended Tetrathiafulvalene Scaffolds for Dye-Sensitized Solar Cells. *Eur. J. Org. Chem.* **2020**, *2020*, 6127–6134. [[CrossRef](#)]
8. Fujiwara, H.; Sugishima, Y.; Tsujimoto, K. Synthesis, structure, and photoelectrochemical properties of new tetrathiafulvalene-diphenyl-1,3,4-oxadiazole dyads. *Tetrahedron Lett.* **2008**, *49*, 7200–7203. [[CrossRef](#)]
9. Fujiwara, H.; Sugishima, Y.; Tsujimoto, K. Synthesis, structure and physical properties of a new TTF derivative containing a PPD part. *J. Phys. Conf. Ser.* **2008**, *132*, 012025. [[CrossRef](#)]
10. Fujiwara, H.; Yokota, S.; Hayashi, S.; Takemoto, S.; Matsuzaka, H. Development of photofunctional materials using TTF derivatives containing a 1,3-benzothiazole ring. *Phys. B* **2010**, *405*, S15–S18. [[CrossRef](#)]
11. Yokota, S.; Tsujimoto, K.; Hayashi, S.; Pointillart, F.; Ouahab, L.; Fujiwara, H. Cu<sup>II</sup> and Cu<sup>I</sup> Coordination Complexes Involving Two Tetrathiafulvalene-1,3-benzothiazole Hybrid Ligands and Their Radical Cation Salts. *Inorg. Chem.* **2013**, *52*, 6543–6550. [[CrossRef](#)]
12. Kishi, Y.; Cornet, L.; Pointillart, F.; Riobé, F.; Lefeuvre, B.; Cador, O.; Le Guennic, B.; Maury, O.; Fujiwara, H.; Ouahab, L. Luminescence and Single-Molecule-Magnet Behaviour in Lanthanide Coordination Complexes Involving Benzothiazole-Based Tetrathiafulvalene Ligands. *Eur. J. Inorg. Chem.* **2018**, *2018*, 458–468. [[CrossRef](#)]
13. Fujiwara, H.; Tsujimoto, K.; Sugishima, Y.; Takemoto, S.; Matsuzaka, H. New fluorene-substituted TTF derivatives as photofunctional materials. *Phys. B* **2010**, *405*, S12–S14. [[CrossRef](#)]
14. Tsujimoto, K.; Ogasawara, R.; Kishi, Y.; Fujiwara, H. TTF-fluorene dyads and their M(CN)<sub>2</sub><sup>−</sup> (M = Ag, Au) salts designed for photoresponsive conducting materials. *New J. Chem.* **2014**, *38*, 406–418. [[CrossRef](#)]
15. Tsujimoto, K.; Ogasawara, R.; Fujiwara, H. Photocurrent generation based on new tetrathiafulvalene-BODIPY dyads. *Tetrahedron Lett.* **2013**, *54*, 1251–1255. [[CrossRef](#)]
16. Tsujimoto, K.; Ogasawara, R.; Nakagawa, T.; Fujiwara, H. Photofunctional Conductors Based on TTF-BODIPY Dyads Bearing *p*-Phenylene and *p*-Phenylenevinylene Spacers. *Eur. J. Inorg. Chem.* **2014**, *2014*, 3960–3972. [[CrossRef](#)]
17. Tang, C.W.; Vanslyke, S.A. Organic Electroluminescent Diodes. *Appl. Phys. Lett.* **1987**, *51*, 913–915. [[CrossRef](#)]
18. Chen, C.H.; Shi, J. Metal chelates as emitting materials for organic electroluminescence. *Coord. Chem. Rev.* **1998**, *171*, 161–174. [[CrossRef](#)]
19. Colle, M.; Dinnebier, R.E.; Brutting, W. The structure of the blue luminescent d-phase of tris(8-hydroxyquinoline)aluminium(III) (Alq<sub>3</sub>). *Chem. Commun.* **2002**, 2908–2909. [[CrossRef](#)]
20. Hung, L.S.; Chen, C.H. Recent progress of molecular organic electroluminescent materials and devices. *Mater. Sci. Eng. R-Rep.* **2002**, *39*, 143–222. [[CrossRef](#)]
21. Ballardini, R.; Varani, G.; Indelli, M.T.; Scandola, F. Phosphorescent 8-quinolinol metal chelates. Excited-state properties and redox behavior. *Inorg. Chem.* **1986**, *25*, 3858–3865. [[CrossRef](#)]
22. Tsuboi, T.; Nakai, Y.; Torii, Y. Photoluminescence of bis(8-hydroxyquinoline) zinc (Znq<sub>2</sub>) and magnesium (Mgq<sub>2</sub>). *Cent. Eur. J. Phys.* **2012**, *10*, 524–528. [[CrossRef](#)]
23. Vivo, P.; Jukola, J.; Ojala, M.; Chukharev, V.; Lemmetyinen, H. Influence of Alq<sub>3</sub>/Au cathode on stability and efficiency of a layered organic solar cell in air. *Sol. Energy Mater. Sol. Cells* **2008**, *92*, 1416–1420. [[CrossRef](#)]
24. Kao, P.-C.; Chu, S.-Y.; Huang, H.-H.; Tseng, Z.-L.; Chen, Y.-C. Improved efficiency of organic photovoltaic cells using tris(8-hydroxy-quinoline) aluminum as a doping material. *Thin Solid Films* **2009**, *517*, 5301–5304. [[CrossRef](#)]
25. Wang, C.S.; Bryce, M.R.; Batsanov, A.S.; Stanley, C.F.; Beeby, A.; Howard, J.A.K. Synthesis, spectroscopy and electrochemistry of phthalocyanine derivatives functionalised with four and eight peripheral tetrathiafulvalene units. *J. Chem. Soc. Perkin Trans.* **1997**, *2*, 1671–1678. [[CrossRef](#)]
26. Parg, R.P.; Kilburn, J.D.; Petty, M.C.; Pearson, C.; Ryan, T.G. A semiconducting Langmuir-Blodgett film of a non-amphiphilic bis-tetrathiafulvalene derivative. *J. Mater. Chem.* **1995**, *5*, 1609–1615. [[CrossRef](#)]
27. Heuzé, K.; Fourmigué, M.; Batail, P.; Canadell, E.; Auban-Senzier, P. Directing the Structures and Collective Electronic Properties of Organic Conductors: The Interplay of  $\pi$ -Overlap Interactions and Hydrogen Bonds. *Chem. Eur. J.* **1999**, *5*, 2971–2976. [[CrossRef](#)]
28. Devic, T.; Avarvari, N.; Batail, P. A Series of Redox Active, Tetrathiafulvalene-Based Amidopyridines and Bipyridines Ligands: Syntheses, Crystal Structures, a Radical Cation Salt and Group 10 Transition-Metal Complexes. *Chem. Eur. J.* **2004**, *10*, 3697–3707. [[CrossRef](#)]
29. Frisch, M.J.; Trucks, G.W.; Schlegel, H.B.; Scuseria, G.E.; Robb, M.A.; Cheeseman, J.R.; Scalmani, G.; Barone, V.; Mennucci, B.; Petersson, G.A.; et al. *Gaussian 09*; Revision B.01; Gaussian, Inc.: Wallingford, CT, USA, 2010.
30. Friedrich, A.; Uhlemann, E.; Weller, F. Chelate von Chinolin-8-ol-Derivaten. XII. Die Kristall- und Molekülstruktur von Bis(7-isopropylchinolin-8-olato)nickel(II). *Z. Anorg. Allg. Chem.* **1992**, *615*, 39–42. [[CrossRef](#)]
31. Xiong, R.-G.; Zou, J.-L.; You, X.-Z.; Wu, Q.-J.; Huang, X.-Y. The synthesis, characterization and crystal structure of trans-bis-(4-methylpyridine)bis(8-quinolinolato-N1,O8)nickel(II)monohydrate. *Transit. Met. Chem.* **1995**, *20*, 498–500. [[CrossRef](#)]

32. Merritt, L.L.; Cady, R.T.; Mundy, B.W. The crystal structure of zinc 8-hydroxyquinolate dihydrate. *Acta Crystallogr.* **1954**, *7*, 473–476. [[CrossRef](#)]
33. Chen, Z.-F.; Zhang, M.; Shi, S.-M.; Huang, L.; Liang, H.; Zhou, Z.-Y. Diaquabis(8-quinolinolato-[kappa]2N,O)zinc(II). *Acta Crystallogr. Sect. E* **2003**, *59*, m814–m815. [[CrossRef](#)]
34. Grice, K.A.; Griffin, G.B.; Cao, P.S.; Saucedo, C.; Niyazi, A.H.; Aldakheel, F.A.; Sterbinsky, G.E.; LeSuer, R.J. Elucidating the Solution-Phase Structure and Behavior of 8-Hydroxyquinoline Zinc in DMSO. *J. Phys. Chem. A* **2018**, *122*, 2906–2914. [[CrossRef](#)] [[PubMed](#)]
35. Zhai, J.; Wei, T.X.; Huang, C.H.; Cao, H. The photoelectrochemical study of a series of ionically combined bischromophore transition metal complexes in LB films. *J. Mater. Chem.* **2000**, *10*, 625–630. [[CrossRef](#)]
36. Nariai, H.; Masuda, Y.; Sekido, E. Structural Characterization of Several Metal(II) 2-Methyl-8-quinolinolato Complexes in Several Organic Solvents. *Bull. Chem. Soc. Jpn.* **1984**, *57*, 3077–3082. [[CrossRef](#)]